To cite this version :

Diana BALTEAN-CARLÈS, Catherine WEISMAN, Philippe DEBESSE, Gurunath GANDIKOTA, Virginie DARU - Two-dimensional numerical simulations of nonlinear acoustic streaming in standing waves - Wave Motion - Vol. 50, p.955-963 - 2013

Two-dimensional numerical simulations of nonlinear acoustic streaming in standing waves

Virginie Daru[a,b], Diana Baltean-Carlès[a,c], Catherine Weisman[a,c], Philippe Debesse[a], Gurunath Gandikota V. S.[a]

[a]*LIMSI-UPR CNRS 3251, BP133, 91403 Orsay Cedex*
[b]*Arts et Métiers ParisTech, Lab. DynFluid, 151 bd de l'hôpital, 75013 Paris*
[c]*Université Pierre et Marie Curie, 4 Place Jussieu, 75252 Paris Cedex 05*

Abstract

Numerical simulations of compressible Navier-Stokes equations in closed two-dimensional channels are performed. A plane standing wave is excited inside the channel and the associated acoustic streaming is investigated for high intensity waves, in the nonlinear streaming regime. Significant distortion of streaming cells is observed, with the centers of streaming cells pushed towards the end-walls. The mean temperature evolution associated to the streaming motion is also investigated.

Keywords: acoustic streaming, standing wave, numerical simulation, nonlinear streaming regime

1. Introduction

Acoustic streaming is generated inside a two-dimensional channel as a consequence of the interaction between a plane standing wave and the solid boundaries. It consists of a mean second order flow produced mainly by shear

---

forces within the viscous boundary layer along the solid walls. This motion was initially studied by Rayleigh [1] in the case of wide channels, in which the boundary layer thickness is negligible in comparison with the channel width. This streaming flow is characterized by four steady counter-rotating vortices outside the boundary layer, nowadays referred to as Rayleigh streaming. The vortices develop along the half wavelength of the standing wave. Along the central axis of the channel, the streaming motion is oriented from acoustic velocity nodes to antinodes. Inside the boundary layer four additional vortices are created simultaneously, with the streaming motion oriented from acoustic velocity antinodes to nodes along the inner walls of the tube [2, 3].

In the case of wide channels, Menguy and Gilbert [4] showed that streaming itself can be linear (case of slow streaming) or nonlinear (case of fast streaming), and both regimes are characterized by a reference nonlinear Reynolds number $Re_{NL} = (M \times y_0/\delta_\nu)^2$ reflecting the influence of inertial effects on the streaming flow (M is the acoustic Mach number, $M = U_{max}/c_0$, with U_{max} the maximum acoustic velocity inside the channel and c_0 the initial speed of sound, y_0 is the half width of the channel and δ_ν the viscous boundary layer thickness). Most analytical streaming models have been established in the case of slow streaming, characterized by $Re_{NL} \ll 1$. They are based on successive approximations of the nonlinear hydrodynamic equations and have been derived for arbitrary values of the ratio y_0/δ_ν, taking into account the variations of heat conduction and viscosity with temperature [5], and the existence of a longitudinal temperature gradient [6]. In the case $Re_{NL} = O(1)$, Menguy and Gilbert [4] derived an asymptotic model for streaming flow inside wide cylindrical resonators, with no mean temperature

2

gradient, and showed a distortion of streaming patterns due to inertia effects. However, this model does not cover the strongly nonlinear streaming regime ($Re_{NL} \gg 1$), and does not explain the nonlinear effects on acoustic streaming recently observed in several experimental works [7, 8, 9], where the temperature gradient along the resonator wall has a significant influence.

Numerical simulations in the linear regime, yielding results for non idealized geometries, were performed in the specific cases of thermoacoustic refrigerators [10] or in annular resonators [11] and solved the dynamics of the flow without taking heat transfer into account.

Simulations in the nonlinear regime were first performed by Yano [12], who studied the acoustic streaming associated with resonant oscillations with periodic shock waves in tubes with aspect ratio (width over length) very large (0.1). He solved the full 2D Navier-Stokes equations with an upwind finite-difference TVD scheme and showed the existence of irregular vortex structures and even turbulent streaming for high streaming Reynolds numbers (based on a characteristic streaming velocity, the tube length, and the kinematic viscosity, $R_s = U_s L/\nu$). This is a different configuration than our configuration, since it considers low frequency acoustic waves in wide tubes with respect to their length and focuses on turbulent streaming.

Simulations of acoustic streaming in the linear and nonlinear regime, taking heat transfer into account, in a two-dimensional rectangular enclosure, were performed by Aktas and Farouk [13]. In their study, the wave is created by vibrating the left wall of the enclosure and the full compressible Navier-Stokes equations are solved, with an explicit time-marching algorithm (a fourth order flux-corrected transport algorithm) to track the acoustic waves.

3

Their numerical results are in agreement with theoretical results in the linear regime and show irregular streaming motion in the nonlinear regime, but they show the existence of irregular streaming at small values of Re_{NL}, in contradiction with experiments cited above. Moreover, these simulations do not analyze the deformation of the streaming cells until they split onto several cells.

We propose in this work to conduct numerical 2D compressible simulations for studying the origin of the distortion of streaming cells (of Rayleigh type) that were experimentally observed. Calculations are performed for channels with aspect ratios ranging from 0.01 to 0.07, and the coupling between streaming effects and thermal effects in the channel (existence of a mean temperature gradient) is also investigated.

2. Problem description and numerical model

We consider a rectangular channel of length L and half width y_0, initially filled with the working gas. In order to initiate an acoustic standing wave in the channel, it is shaken in the longitudinal direction (x), so that an harmonic velocity law is imposed, $\mathbf{V}(t) = (V(t), 0)^T$, with $V(t) = x_p \omega \cos(\omega t)$, ω being the angular frequency and x_p the amplitude of the channel displacement. The channel being undeformable, the flow can be modeled by the compressible Navier-Stokes equations expressed in the moving frame attached to the

4

channel, so that a forcing source term is added. The model reads:

$$
\begin{cases}
\dfrac{\partial \rho}{\partial t} + \nabla \cdot (\rho \mathbf{v}) &=& 0 \\[2mm]
\dfrac{\partial \rho \mathbf{v}}{\partial t} + \nabla \cdot (\rho \mathbf{v} \otimes \mathbf{v}) + \nabla p &=& \nabla \cdot (\bar{\bar{\tau}}) - \rho \dfrac{d\mathbf{V}}{dt} \\[2mm]
\dfrac{\partial \rho E}{\partial t} + \nabla \cdot (\rho E \mathbf{v} + p\mathbf{v}) &=& \nabla \cdot (k\nabla T) + \nabla \cdot (\bar{\bar{\tau}}\mathbf{v}) - \rho \mathbf{v} \cdot \dfrac{d\mathbf{V}}{dt}
\end{cases}
\tag{1}
$$

where $\mathbf{v} = (u, v)^T$ is the flow velocity, $E = e + \frac{1}{2}\mathbf{v} \cdot \mathbf{v}$ is the total energy, with $e = \frac{p}{(\gamma-1)\rho}$ the internal energy, γ the specific heat ratio, $\bar{\bar{\tau}} = -\frac{2}{3}\mu(\nabla \cdot \mathbf{v})\bar{\bar{I}} + 2\mu\bar{\bar{D}}$ the viscous stress tensor of a Newtonian fluid, $\bar{\bar{D}}$ the strain tensor, μ the dynamic viscosity, k the thermal conductivity. The thermo-physical properties μ and k are supposed to be constant. The gas is considered as a perfect gas obeying the state law $p = r\rho T$, where T is the temperature and r is the perfect gas constant corresponding to the working gas. The physical boundary conditions employed in the moving frame are: no slip and isothermal walls.

The model is numerically solved by using high order finite difference schemes, developed in Daru and Tenaud [14]. An upwind scheme, third order accurate in time and space, is used for convective terms, and a centered scheme, second order, is used for diffusion terms. More detail about the scheme and computations showing its good qualities can be found in Daru and Gloerfelt [15], Daru and Tenaud [16]. This scheme can be derived up to an arbitrary order of accuracy for convective terms in the case of a scalar equation. Here the third order scheme is selected, after having done several comparisons using higher order schemes (up to the 11th order), that have shown that third order gives sufficient accuracy for a reasonable CPU cost. In cases where shock waves are present, the scheme can be equipped

5

with a flux limiter (MP), preserving monotonicity, intended for suppressing the parasitic numerical oscillations generated in the shock region, while preserving the accuracy of the scheme in smooth regions. However, the flows considered here are always low Mach number flows. Although traveling shock waves are a main feature of the flow for high acoustics levels, as noticed by several authors [17], they are of weak intensity and the numerical oscillations are very small and do not spoil the solution. Thus the MP limiter, which is expensive in terms of CPU cost, was not activated in these calculations. For solving the 2D Navier-Stokes equations, the scheme is implemented using Strang splitting. This reduces the formal accuracy of the scheme to second order. However, numerical experiments have shown that a very low level of error is still achieved.

Let us describe our numerical procedure. The system (1) can be written in vector form :

$$\frac{\partial w}{\partial t} + \frac{\partial}{\partial x}(f - f^v) + \frac{\partial}{\partial y}(g - g^v) = h \qquad (2)$$

where w is the vector of conservative variables $(\rho, \rho u, \rho v, \rho E)^T$, f and g are the inviscid fluxes $f = (\rho u, \rho u^2 + p, \rho uv, \rho Eu + pu)^T$ and $g = (\rho v, \rho uv, \rho v^2 + p, \rho Ev + pv)^T$, f^v and g^v being the viscous fluxes $f^v = (0, \tau_{xx}, \tau_{xy}, k\frac{\partial T}{\partial x} + u\tau_{xx} + v\tau_{xy})^T$, $g^v = (0, \tau_{xy}, \tau_{yy}, k\frac{\partial T}{\partial y} + u\tau_{xy} + v\tau_{yy})^T$. The source term reads $h = (0, -\rho\frac{dV}{dt}, 0, -\rho u\frac{dV}{dt})^T$. Denoting $w_{i,j}^n$ the numerical solution at time $t = n\delta t$ and grid point $(x, y) = (i\delta x, j\delta y)$, we use the following Strang splitting procedure to obtain second order of accuracy every two time steps :

$$w_{i,j}^{n+2} = L_{\delta x} L_{\delta y} L_{\delta y} L_{\delta x} w_{ij}^n \qquad (3)$$

where $L_{\delta x}$ (resp. $L_{\delta y}$) is a discrete approximation of $L_x(w) = w + \delta t(-f_x +$

118    $f^v_x + h)$ (resp. $L_y(w) = w + \delta t(-g_y + g^v_y))$. The 1D operators being similar

119   in the two directions, we only describe the x operator. The scheme is imple-

120   mented as a correction to the second order MacCormack scheme. It consists

121   of three steps, as follows :

$$
\begin{aligned}
w^*_{i,j} &= w^n_{i,j} - \tfrac{\delta t}{\delta x}(f_{i+1,j} - f_{i,j} - f^v_{i+1/2,j} + f^v_{i-1/2,j})^n + \delta t\ h^n_{i,j} \\
w^{**}_{i,j} &= w^*_{i,j} - \tfrac{\delta t}{\delta x}(f_{i,j} - f_{i-1,j} - f^v_{i+1/2,j} + f^v_{i-1/2,j})^* \qquad (4) \\
w^{n+1}_{i,j} &= \tfrac{1}{2}(w^n_{i,j} + w^{**}_{i,j}) + C^x_{i+1/2,j} - C^x_{i-1/2,j}
\end{aligned}
$$

122   The viscous fluxes are discretized at each interface using centered second or-

123   der finite differences formulae. The corrective term $C^x_{i+1/2,j} - C^x_{i-1/2,j}$ provides

124   the third order accuracy and the upwinding for the inviscid terms. Let us de-

125   fine $\psi_{i+1/2,j} = \tfrac{1}{6}\sum_{l=1}^{4}\left\{|\nu^l_{i+1/2,j}|(1 - \nu^l_{i+1/2,j})(1 + \nu^l_{i+1/2,j})\delta\alpha^l_{i+1/2,j} \cdot d^l_{i+1/2,j}\right\}$,

126   where $\nu^l = \tfrac{\delta t}{\delta x}\lambda^l$, λ^l and d^l are the eigenvalues and eigenvectors of the Roe-

127   averaged jacobian matrix $A = \tfrac{df}{dw}$ [18], and $\delta\alpha^l$ is the contribution of the

128    $l-$wave to the variation $(w^n_{i+1/2,j} - w^n_{i-1/2,j})$. Using the function ψ, the cor-

129   rective term reads :

$$
C^x_{i+1/2,j} = \begin{cases} -\psi^n_{i+1/2,j} + \psi^n_{i-1/2,j} & if \quad \nu_{i+1/2,j} \geq 0 \\ \psi^n_{i+3/2,j} - \psi^n_{i+1/2,j} & if \quad \nu_{i+1/2,j} < 0 \end{cases} \qquad (5)
$$

130   This completes the description of the numerical method.

131   We are interested in the acoustic streaming generated by the interaction of

132   the imposed plane standing wave and the channel wall. Resonant conditions

133   are imposed, for which $L = \lambda/2$, $\lambda = c_0/f$ being the wave length, c_0 the speed

134   of sound for initial state and f the vibration frequency of the channel. It is

135   known [5] that boundary layers develop along the walls, with thickness $\delta_\nu =$

136    $\sqrt{2\nu/\omega}$, ν being the kinematic viscosity $\nu = \mu/\rho_0$, and ρ_0 the density at initial

137   state. Depending on the value of the ratio y_0/δ_ν, several patterns of streaming

can appear: Rayleigh-type streaming in the central region, and boundary layer type streaming near the longitudinal walls. The boundary layer is of small thickness and must be correctly resolved by the discretization mesh. After several trials, we have determined that a value of 5 points per boundary layer thickness is sufficient for reasonable accuracy of the simulations. The results obtained using 10 points per boundary layer thickness show very small differences with the former, the maximum value of the differences being less than 3%. All results presented below are thus obtained using a cartesian mesh of rectangular cells of constant size δx and δy, composed of 500 points in the axial direction x, and of $5 \times y_0/\delta_\nu$ points in the y direction normal to the axis. In the considered geometry, this leads to cells such that $\delta y \ll \delta x$. The flow being symmetrical with respect to the x axis (at least in the range of parameters treated), only the upper half of the channel was considered. Also, the scheme being fully explicit, the time step δt is fixed such as to satisfy the stability condition of the scheme which can be written as:

$$\delta t \leq \frac{1}{2}\min(\delta y^2/\nu, \delta y^2/(k/\rho_0 c_0), \delta y/c_0) \tag{6}$$

As shown in Equation (6), the first two limiting values $\delta y^2/\nu$ and $\delta y^2/(k/\rho_0 c_0)$ are related to the viscous and thermal conduction terms, and the third one $\delta y/c_0$ is related to the acoustic propagation. In all cases considered here, the time step limitation is acoustic, ie $\delta t \leq \frac{1}{2}\delta y/c_0$. Taking $\delta t = \frac{1}{2}\delta y/c_0$ and $\delta y = \delta_\nu/5$, this results in a number of time steps N_T per period of oscillation proportional to $\sqrt{L}$, $N_T = 1/(f\delta t) = 10\sqrt{\frac{2\pi c_0}{\nu}}\sqrt{L}$. Since transients of several hundreds of periods may be needed in order to reach stabilized steady streaming flow, simulations are very costly, and one must rely on numerical schemes that are sufficiently accurate in both space and time.

8

Finally, the mean flow is obtained from calculating a simple mean value for each physical quantity (velocity, pressure, temperature) over an acoustic period. The mean velocity obtained is the so-called Eulerian streaming velocity. The Lagrangian streaming velocity, associated to the streaming mass transport, could also be computed. The difference between them is significant only in the boundary layer, and in the case of wide channels the two velocities are almost the same. In order to observe the mechanism of cell distortion, either one of these velocities can be monitored.

3. Numerical results

We consider a channel initially filled with air at standard thermodynamic conditions, $p_0 = 101325$Pa, $\rho_0 = 1.2$kgm^{-3}, $T_0 = 294.15$K. The thermo-physical properties of air are $\mu = 1.795 \; 10^{-5}$kgm^{-1}s^{-1} and $k = 0.025$Wm^{-1}K^{-1}. Also for air, $\gamma = 1.4$ and $r = 287.06$Jkg^{-1}K^{-1}. The Prandtl number Pr is equal to 0.726. This results in an initial speed of sound $c_0 = 343.82$ms^{-1}.

For a 1m long channel, the limiting time step would correspond to $N_T \approx 25000\sqrt{L}$, that is 25000 iterations per period. Since transients of several hundreds of periods may be needed in order to reach stabilized streaming flow, several millions of iterations are necessary for each simulation. Considering these numerical constraints, a shorter channel is considered, with $L = 8.59$mm. This corresponds to a high-frequency wave, with $f = 20000$Hz. The resulting boundary layer thickness is $\delta_\nu = 1.54 \; 10^{-5}$m. The time step $\delta t = 8 \; 10^{-9}$s is chosen in order to satisfy the numerical stability condition, corresponding to 6250 time iterations per period for a mesh involving 5 grid

9

$x_p(\mu m)$	5	10	50	80	100
$U_{max}(m/s)$	7.0	26.45	61.11	70.94	89.96
y_0/δ_ν	10	40	20	10	20
y_0/L	0.0180	0.0718	0.0359	0.018	0.0359
Re_{NL}	0.041	9.469	12.636	4.257	27.384

Table 1: Values of the parameters of the simulations.

points across the boundary layer thickness. The acoustic velocity produced in the channel depends on the amplitude of the channel displacement and on the ratio y_0/δ_ν. It varies approximately linearly with the amplitude of the channel displacement, for a given ratio y_0/δ_ν. Table 1 summarizes the different parameter values corresponding to the simulations that are presented thereafter.

As mentioned earlier, the parameter identified as relevant in describing the regularity of streaming flow is the nonlinear Reynolds number Re_{NL} introduced by Menguy and Gilbert [4]. In this paper we used a slightly different definition for Re_{NL}, because the definition of the viscous boundary layer thickness is different. Our Reynolds number corresponds to half of that of Menguy and Gilbert [4].

We first present results concerning the main acoustic field in the channel, for a small value of Re_{NL} corresponding to slow streaming. In Figure 1(a) is represented the velocity signal at the center of the channel, as a function of the number of periods elapsed. At this location, the acoustic velocity amplitude is maximum since it corresponds to the antinode. For this value of Re_{NL}, the problem is nearly linear and the final signal is purely sinu-

soidal, in agreement with the linear theory. The amplification of the initial perturbation until saturation can be observed. The periodic regime is established after about 20 periods. Figure 1(b) shows the time evolution of the mean horizontal velocity (over an acoustic period) and of the mean temperature difference $\Delta T = T - T_0$ (also over an acoustic period) on the axis, at $x = \lambda/8$. At this location the streaming velocity is maximum. It can be noticed that the steady streaming field is established also after about 20 periods which is of the same order of magnitude as the theoretical characteristic streaming time scale $\tau_c = (\frac{2y_0}{\pi})^2 \frac{1}{\nu}$, (see Amari, Gusev and Joly [19]) which in this case gives n_c periods for reaching steady-state, with $n_c = 13$. In Figure 2(a) is shown the variation of the axial dimensionless streaming velocity at $x = \lambda/8$ along the channel's width, compared with results computed using the analytical expressions of Hamilton, Ilinskii and Zabolotskaya [20]. In this figure, the reference velocity is the Rayleigh streaming reference velocity [2, 5], $u_{Rayleigh} = \frac{3}{16}U_{max}^2/c_0$. The slight discrepancy between the numerical and the analytical profiles is probably due to the presence of the vertical end walls, which is not accounted for in the model of Hamilton, Ilinskii and Zabolotskaya [20]. In Figure 2(b) is shown the stabilized mean pressure $p - p_0$ (over an acoustic period), scaled by $(\gamma/4)p_0 M^2$, along the channel's axis. It is the second order average pressure resulting from the streaming flow, which is clearly one-dimensional and has a cosine variation with respect to x, as expected in the linear regime of streaming. In the present case, there is an offset pressure p_{off}, corresponding to an increase of the mean pressure and temperature (uniform in space) inside the channel, due to the harmonic forcing source term. When subtracting off this offset pressure, the theoretical
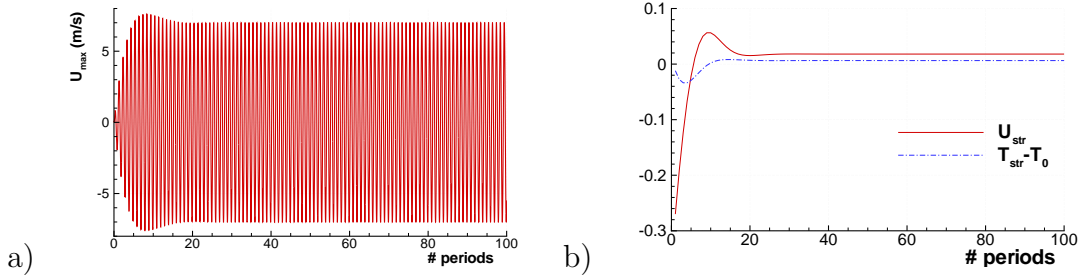
11

Figure 1: a) Acoustic velocity at the channel's center, as a function of time counted by the number of periods elapsed. b) Mean horizontal velocity and mean temperature variation, on the channel's axis at $x = \lambda/8$. Case $Re_{NL} = 0.041$ ($y_0/\delta_\nu = 10$, $M = 0.02$).
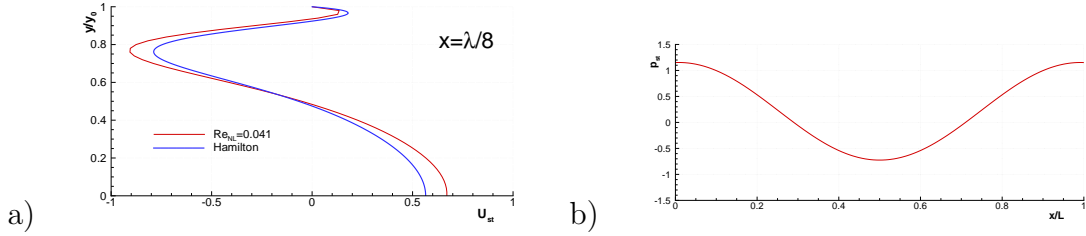

Figure 2: a) U_{st} as a function of y/y_0 at $x = \lambda/8$, numerical (present study) and analytical [20] results. b) Dimensionless mean fluctuating pressure, $p - p_0$ along the channel's axis. Case $Re_{NL} = 0.041$ ($y_0/\delta_\nu = 10$, $M = 0.02$).

result for the dimensionless hydrodynamic streaming pressure is obtained,

$P_{2s} = \cos 4\pi \frac{x}{\lambda}$ (see Menguy and Gilbert [4]).

Simulations are then performed for several values of Re_{NL} corresponding to configurations ranging from slow streaming flow ($Re_{NL} = 0.041$) to fast streaming flow ($Re_{NL} = 27.384$), for several values of the cavity width ($y_0/\delta_\nu = 10, 20, 40$), and for increasing acoustic velocities, with Mach numbers ranging from $M = 0.02$ to $M = 0.27$ so that shock waves can occur. This can be seen in Figure 3(right) showing the acoustic velocity signal at channel's center as a function of time counted by the number of periods

elapsed. In Figure 3(a)(right) the signal contains only one frequency, but for all other cases, there are shock waves and the acoustic velocity signal is distorted in a "U" shape, because of the presence of odd harmonics (3, 5, etc). Figure 3(left) shows the streamlines of the streaming velocity field over the whole length and only over the top half width of the channel. As expected, in the case of small Re_{NL} number values (Figure 3(a)), four symmetric streaming cells develop over the length and the half width of the channel: two cells in the boundary layer, and two cells in the core of the channel, identified in the literature as Rayleigh streaming. These results are in agreement with the predictions of analytical models of streaming flows [5, 6], and with experimental measurements [7]. The only noticeable difference is the slight asymmetry of cells with respect to the vertical lines $x = \lambda/8$ and $x = 3\lambda/8$, due to the presence of vertical boundary layers. Indeed these boundary layers are accounted for in the present simulations but are neglected in the analytical models, and are very far from the measurement area in the experiments. Several simulations have shown that this asymmetry is independent of Re_{NL} as long as the value of the latter remains small with respect to 1.

For $Re_{NL} > 1$, the steady streaming flow is established after the same characteristic time as in the linear case. The recirculation cells become very asymmetric as Re_{NL} increases, and streaming flow becomes irregular (Figure 3(b,c,d,e)(left)). This was also observed experimentally (with PIV measurements) by Nabavi, Siddiqui and Dargahi [8] in a rectangular enclosure. The centers of all streaming cells (boundary layer cells as well as central cells) are displaced towards the ends of the resonant channel, close to the boundary layers next to the vertical walls. PIV measurements by Nabavi,

13

Siddiqui and Dargahi [8] show the same distortion of streamlines between an acoustic velocity node and an antinode. Figure 4(a) shows the x variation along the channel's central axis $y = 0$, of the axial dimensionless streaming velocity component, using as reference velocity the Rayleigh streaming reference velocity [2, 5], $u_{Rayleigh} = \frac{3}{16} U_{max}^2 / c_0$. There is a clear modification of the velocity profiles as Re_{NL} increases: the sine function associated to slow streaming becomes steeper next to the channel's ends. The slope to the curve at the channel's center (acoustic velocity node) becomes smaller as Re_{NL} increases, then becomes close to zero (curve parallel to the longitudinal axis) for a critical value between 13 and 27, and then changes sign, which indicates the emergence of new streaming cells (Figure 4(a)). Another consequence of the distortion of streaming cells can be observed on the acoustic streaming axial velocity profiles along the width of the channel, shown in Figure 4(b,c,d). The parabolic behavior in the center of the channel at $x = \lambda/8$ disappears as Re_{NL} increases (see Figure 4(b)), as a consequence of displacement of the center of each streaming cell toward the velocity node. Figures 4(c,d) also confirm the direction of the displacement of the streaming cells' centers. This distortion of streaming cells was already observed in experiments in rectangular or cylindrical geometries in wide channels [7, 8, 9]. Nabavi, Siddiqui and Dargahi [8] described it as irregular streaming and detected a critical nonlinear Reynolds number $Re_{NL} = 25$ that separates regular and irregular streaming, which is in agreement with our simulations. In the literature there is to our knowledge no other theoretical or numerical study confirming measurements in these streaming regimes. With the weakly nonlinear model of Menguy and Gilbert [4] the streaming can be calculated for a maximum

14

value of $Re_{NL} = 2$ (in our definition), while the numerical simulations of Aktas and Farouk [13] show the existence of multiple streaming cells for a low value of $Re_{NL} = 1.4$, which is in contradiction with our results and with experiments. Moreover, these numerical simulations [13] do not analyse in detail the transition from two exterior streaming cells to more streaming cells.

According to Menguy and Gilbert [4], the fluid inertia causes distortion of streaming cells for large values of Re_{NL}. This was also verified through our simulations. For $Re_{NL} = O(1)$, the Mach number is still small (the wave is almost a mono-frequency wave) and the mean temperature difference inside the channel is smaller than 0.1K (the mean temperature gradient is negligible). The approximations of the model by Menguy and Gilbert [4] still apply here, so we can say that the distortion is caused only by inertial effects. When Re_{NL} increases, periodic shocks appear and the mean temperature gradient becomes important in our simulations. In their experimental study, Thompson, Atchley and Maccarone [9] show the existence of some distortion of the streaming field that are not predicted by existing models of the literature in the nonlinear regime. They do not relate this distortion to fluid inertia but rather to the influence of the mean temperature field, and more specifically of the axial temperature gradient induced through a thermoacoustic effect along the horizontal walls of the resonating channel. In an experimental case with no shock waves, Merkli and Thomann [17] showed that a mean temperature gradient is established inside the tube so that heat is removed close to the velocity antinodes, i.e. at the location of largest viscous dissipation, and heat is produced close to velocity nodes, along the lateral walls. Similar
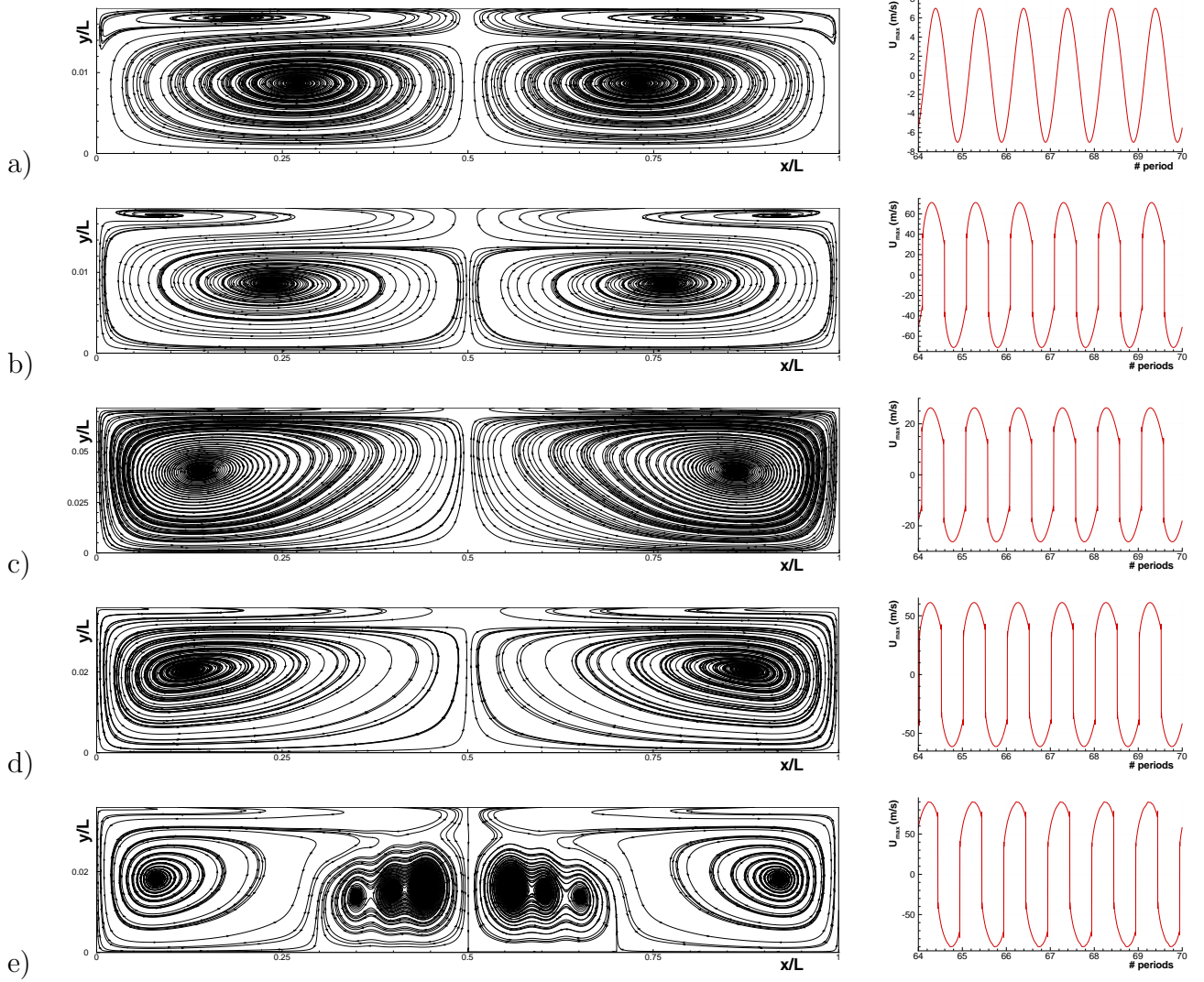
Figure 3: Streamlines of mean flow on the top half of the channel (left) and acoustic velocity signal at channel's center as a function of time counted by the number of periods elapsed (right) a) $Re_{NL} = 0.041$ ($y_0/\delta_\nu = 10$, $M = 0.02$). b) $Re_{NL} = 4.257$ ($y_0/\delta_\nu = 10$, $M = 0.206$). c) $Re_{NL} = 9.469$ ($y_0/\delta_\nu = 40$, $M = 0.077$). d) $Re_{NL} = 12.636$ ($y_0/\delta_\nu = 20$, $M = 0.178$). e) $Re_{NL} = 27.384$ ($y_0/\delta_\nu = 20$, $M = 0.262$). Lengths are normalized with L.
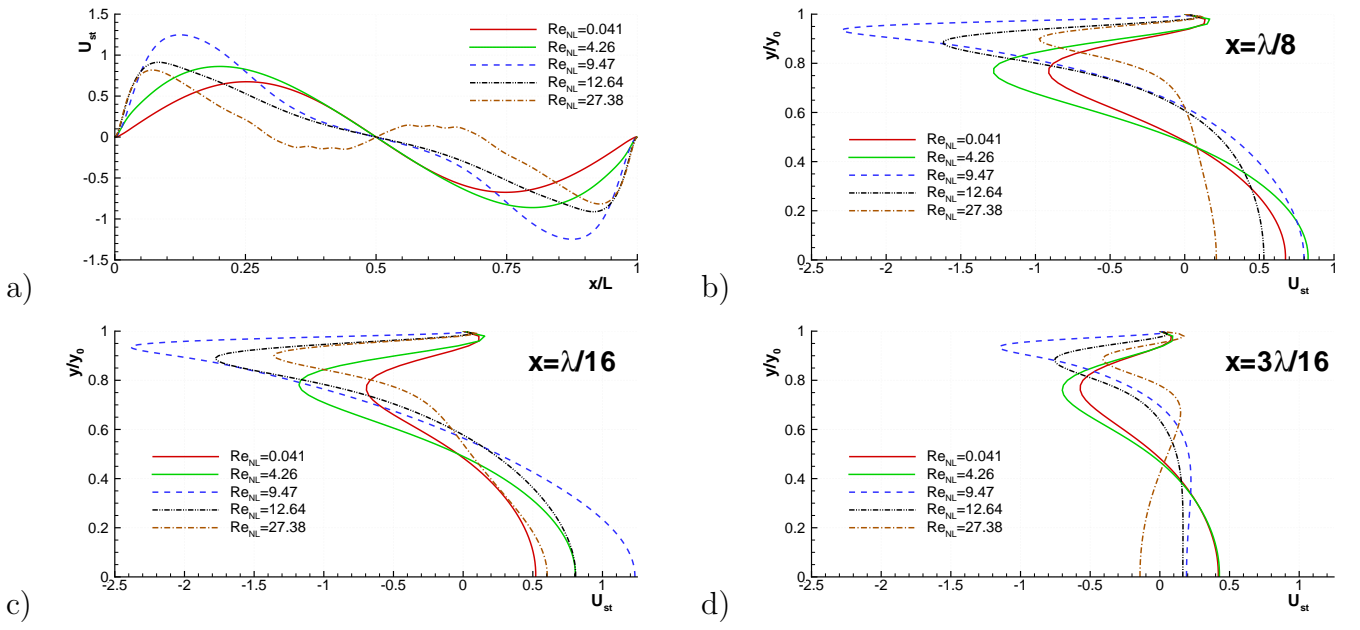
Figure 4: Horizontal mean velocity component U_{st}, normalized with $\frac{3}{16}U_{max}^2/c_0$ for the 5 cases of Figure 3. a) U_{st} along the channel's central axis. b),c) and d) U_{st} as a function of y/y_0 for several sections x.
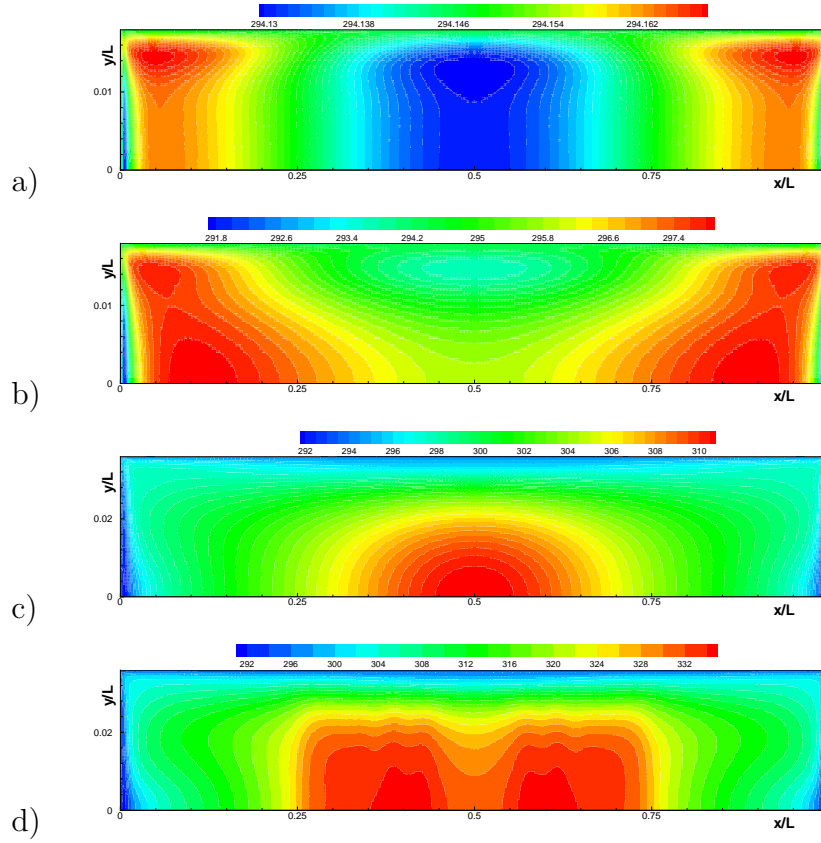
17

Figure 5: Mean temperature field on the top half of the channel, a) $Re_{NL} = 0.041$. b) $Re_{NL} = 4.257$. c) $Re_{NL} = 12.636$. d) $Re_{NL} = 27.383$. The difference between minimum and maximum values of temperature is (respectively) : a) $\Delta T = 0.039$K, b) $\Delta T = 6.39$K, c) $\Delta T = 19.4$K, d) $\Delta T = 44$K.

observations can be made in our simulations as seen in Figure 5(a) which shows the mean temperature field for small values of Re_{NL}. The thermoacoustic heat transport takes place at a distance of one thermal boundary layer thickness and then heat diffuses in the radial direction, yielding a temperature field almost one-dimensional in the central part of the tube in the steady-state. As Re_{NL} increases however, the mean temperature field clearly becomes two-dimensional, as a consequence of both convective heat transport by streaming flow and heat conduction in both directions (Figure 5(b)). Within the considered range of values of the nonlinear Reynolds number, there is a change of regime for the temperature field before $Re_{NL} = 13.26$, corresponding to the confinement of outer streaming cell towards the acoustic velocity node. Consequently a zone of very small streaming velocities is generated in the middle of the cavity and that induces the accumulation of heat (Figure 5(c)). The mean temperature gradient changes the orientation and can cause the splitting of the outer cell into several cells when further increasing Re_{NL} (Figure 5(d)).

Note that the streaming flow stabilizes in several stages in regimes with high values of the nonlinear Reynolds number. In a first and rapid stage (a few tens of periods), regular streaming flow appears. Then this regular streaming is destabilized along with increasing heterogeneity of the mean temperature field. The steady mean flow stabilizes much later, with time scales related to convection and heat conduction.

19

4. Conclusions

The numerical simulations performed demonstrate the transition from regular acoustic streaming flow towards irregular streaming, in agreement with existing experimental data. These are the first simulations, to our knowledge, in good alinement with experiments of nonlinear streaming regimes. Results show a sizable influence of vertical boundary layers for the chosen configuration. There is also intricate coupling between the mean temperature field and the streaming flow. This coupling effect will be the object of future work. Also, extension of current results in configurations with larger channels is currently in progress.

Acknowledgements

References

[1] Lord Rayleigh, On the circulation of air observed in Kundts tubes, and on some allied acoustical problems, Philos. Trans. R. Soc. London 175 (1884) 1-21.

[2] W.L. Nyborg, Acoustic streaming, in Physical Acoustics, W. P. Mason (ed), Academic Press, New York Vol. 2B (1965) 265-331.

[3] H. Schlichting, Berechnung ebener periodischer Grenzschicht- strommungen [calculation of plane periodic boundary layer streaming], Phys. Zcit. 33 (1932) 327-335.

[4] L. Menguy, J. Gilbert, Non-linear Acoustic Streaming Accompanying a Plane Stationary Wave in a Guide, Acta Acustica 86 (2000) 249-259.

[5] M.F. Hamilton, Y.A. Ilinskii, E.A. Zabolotskaya, Acoustic streaming generated by standing waves in two-dimensional channels of arbitrary width, J. Acoust. Soc. Am. 113(1) (2003) 153-160.

[6] H. Bailliet, V. Gusev, R. Raspet, R.A. Hiller, Acoustic streaming in closed thermoacoustic devices, J. Acoust. Soc. Am. 110 (2001) 1808-1821.

[7] S. Moreau, H. Bailliet, J.-C. Valière, Measurements of inner and outer streaming vortices in a standing waveguide using laser doppler velocimetry, J. Acoust. Soc. Am. 123(2) (2008) 640-647.

[8] M. Nabavi, K. Siddiqui, J. Dargahi, Analysis of regular and irregular acoustic streaming patterns in a rectangular enclosure, Wave Motion 46 (2009) 312-322.

[9] M.W. Thompson, A.A. Atchley, M.J. Maccarone, Influences of a temperature gradient and fluid inertia on acoustic streaming in a standing wave, J. Acoust. Soc. Am. 117(4) (2004) 1839-1849.

[10] D. Marx, P. Blanc-Benon, Computation of the mean velocity field above a stack plate in a thermoacoustic refrigerator, C.R. Mecanique 332 (2004) 867-874.

[11] A. Boufermel, N. Joly, P. Lotton, M. Amari, V. Gusev, Velocity of Mass Transport to Model Acoustic Streaming: Numerical Application to Annular Resonators, Acta Acust. United Acust. 97(2) (2011) 219-227.

[12] T. Yano, Turbulent acoustic streaming excited by resonant gas oscillation with periodic shock waves in a closed tube, J. Acoust. Soc. Am. 106 (1999) L7-L12.

[13] M.K. Aktas, B. Farouk, Numerical simulation of acoustic streaming generated by finite-amplitude resonant oscillations in an enclosure, J. Acoust. Soc. Am. 116(5) (2004) 2822-2831.

[14] V. Daru, C. Tenaud, High Order One-step Monotonicity-Preserving Schemes for Unsteady Compressible flow Calculations, Journal of Computational Physics 193 (2004) 563- 594.

[15] V. Daru, X. Gloerfelt, Aeroacoustic computations using a high order shock-capturing scheme, AIAA Journal 45(10) (2007) 2474-248.

[16] V. Daru, C. Tenaud, Numerical simulation of the viscous shock tube problem by using a high resolution monotonicity preserving scheme, Computers and Fluids 38(3) (2009) 664-676.

[17] P. Merkli, H. Thomann, Thermoacoustic effects in a resonance tube, J. Fluid Mech. 70(1) (1975) 161-177.

[18] P.L. Roe, Approximate Riemann solvers, parameter vectors and difference schemes, Journal of Computational Physics, 43 (1981) 357-372.

[19] M. Amari, V. Gusev, N. Joly, Temporal dynamics of the sound wind in acoustitron, Acta Acustica united with Acustica 89 (2003) 1008-1024.

[20] M.F. Hamilton, Y.A. Ilinskii, E.A. Zabolotskaya, Thermal effects on

401   acoustic streaming in standing waves, J. Acoust. Soc. Am. 114(6) (2003)

402   3092-3101.